ORNL/TM-2022/2511
Final CRADA – NFE-19-07529

# High Performance Computing to Quantify the Evolution of Microscopic Concentration Gradients During Flash Processing


Balasubramaniam Radhakrishnan
Younggil Song
Sarma Gorti
Gary Cola

**August 2022**

OAK RIDGE National Laboratory

ORNL IS MANAGED BY UT-BATTELLE LLC FOR THE US DEPARTMENT OF ENERGY

**ORNL/TM-2022/2511**
**Final CRADA – NFE-19-07529**

HPC4EI Report

# HIGH PERFORMANCE COMPUTING TO QUANTIFY THE EVOLUTION OF MICROSCOPIC CONCENTRATION GRADIENTS DURING FLASH PROCESSING

Balasubramaniam Radhakrishnan and Sarma Gorti
Computational Sciences and Engineering Division, Oak Ridge National Laboratory
Younggil Song, Lawrence Livermore National Laboratory
Gary Cola, SFP Works, LLC

August 2022

Prepared by
OAK RIDGE NATIONAL LABORATORY
Oak Ridge, TN 37831
managed by
UT-BATTELLE LLC
for the
US DEPARTMENT OF ENERGY
under contract DE-AC05-00OR22725

**CONTENTS**

## LIST OF FIGURES

## LIST OF TABLES

## ABSTRACT

During the Flash process, the cross section of a plain-carbon or a low-alloy steel is austenitized through rapid heating and transformed on rapid cooling to a predominantly martensite + bainite structure with small amounts of retained austenite. Unlike conventional heat treating, homogeneity is intentionally avoided during Flash processing of steels. The Flash process assembly consists of a pair of rolls that transfer the steel sheets through the heating and cooling stage of the thermal cycle. The initial microstructure of the steel consists of ferrite (body-centered cubic iron) + carbide ((Fe,X)mCn) mixture. The heating rate through the peak temperature is a function of temperature and reaches a peak of about 300-400°C/s and the cooling rate has a maximum value of 3,000-4,000°C/s. The on-heating phase transformations include carbide dissolution, austenite (face-centered cubic iron) nucleation and growth, and diffusion of carbon and other substitutional elements in the steel. The on-cooling phase transformations include formation of martensite (body-centered tetragonal phase containing supersaturated solute) and bainite (ferrite plates with or without fine carbides). In this project, the focus is on Fe-C-Cr steels that are currently Flash processed for armor applications. The modeling effort proposed here will help optimize the Flash thermal cycle for these low alloy steels to achieve the target performance, which is an ongoing effort at SFP Works. A significant feature of Flash processed Fe-C-Cr steels is the presence of scatter in the through-thickness in the sheet. The variability in hardness results from a variability in the bainite + martensite microstructure that is sensitive to the local chemical concentration of C and Cr. Such a chemical inhomogeneity is intentionally obtained in the Flash process. Although such a microstructural gradient is presumably responsible for the exceptional properties of the Flash processed steel, it is very important to quantify the gradients as a function of Flash variabilities in processing parameters and the input microstructure. Understanding the mechanistic pathway that leads to microstructural gradients could be ground-breaking and instrumental for achieving better process control and optimized microstructural state to meet application-specific strength-ductility requirements. Since the final microstructure depends on setting up precise solute concentration gradients through a rapid heating process, and transforming these regions into various phases, it is important to understand how small changes in steel chemistry, input microstructure (carbide size and distribution), and process variables (Flash thermal cycle) will impact the solute concentration gradients.

# 1. INTRODUCTION

A schematic set-up of the Flash process is shown in Figure 1. The assembly consists of a pair of rolls that transfer the steel sheets through the heating and cooling stage of the thermal cycle as shown in Figure 1. Typical microstructures before and after Flash processing are shown in Figure 2. The microstructure prior to Flash processing consists of a ferrite matrix with a mean grain size of 10$\mu$m with a distribution of spheroidized carbide particles. The microstructure after Flash processing is composed of a mixture of martensite, bainite, and retained austenite. Ideally a microstructure consisting of about 80% martensite and 20% bainite is targeted after Flash processing [1]. The strength (1100 to 2100 MPa) and ductility (9-11% elongation) put these steels in the category of Advanced High Strength Steels (AHSS) with successful applications in automotive and defense sectors with a significantly reduced processing cost compared to AHHS made by conventional industrial practice [2]. The hardness scatter in the through-thickness section in a Flash processed Fe-C-Cr steel is shown in Figure 3 [3]. The variability in hardness results from a variability in the bainite + martensite microstructure that is sensitive to the local chemical concentration of C and Cr. The computational goal of this project is to perform mesoscale simulations to capture the generation of concentration gradients occurring during the on-heating portion, and the on-cooling portion of the Flash processing cycle prior to the onset of the bainitic and martensitic transformation. Predicting the local concentration gradients at the mesoscale is an important first step in predicting the distribution of the bainite and martensitic phases in the final microstructure. The microstructural events include grain growth, dissolution of carbides and the coupling between the two phenomena, the nucleation and growth of austenite either in inhomogeneous ferrite, or at the carbide-ferrite interface, and further evolution of concentration gradients in austenite prior to the final bainite or martensite transformation. The local environment of the dissolving carbide could be either a grain boundary of a specific type or the interior of a ferrite grain.

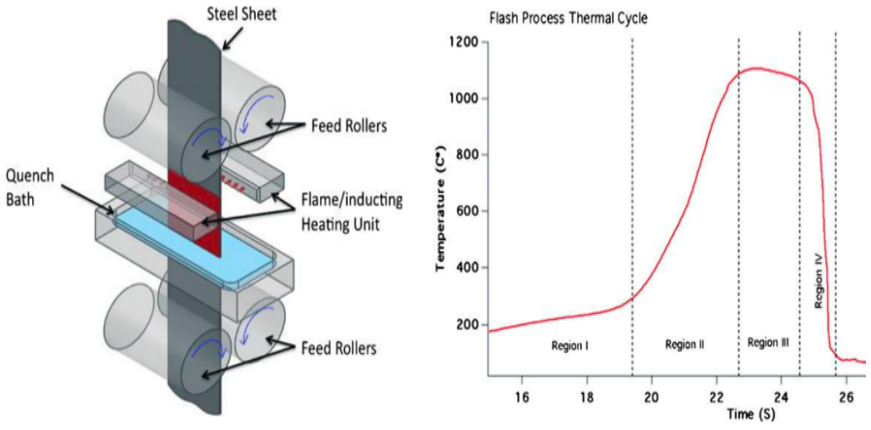


**Figure 1. Schematic of the Flash process (left) and a typical Flash thermal cycle (right)**

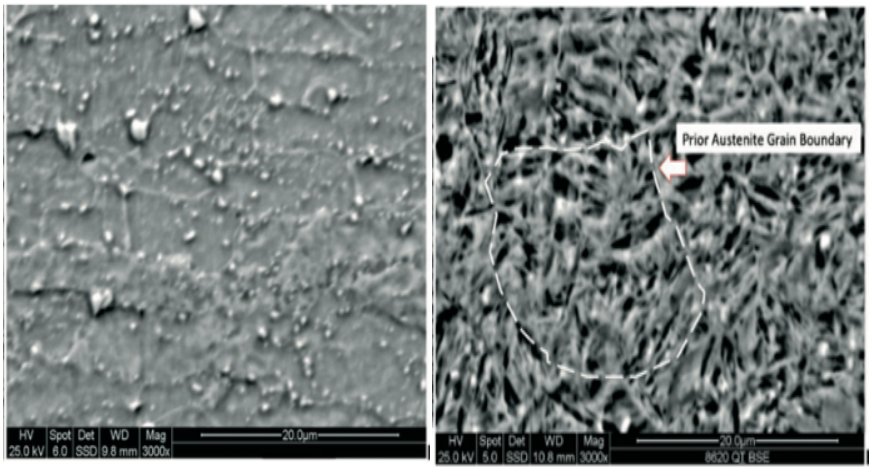


**Figure 2. Typical microstructure of a Fe-Cr-C steel before Flash processing showing distribution of carbides in ferrite grains (left), microstructure after flash processing showing mixture of martensite and bainite (right). [3]**

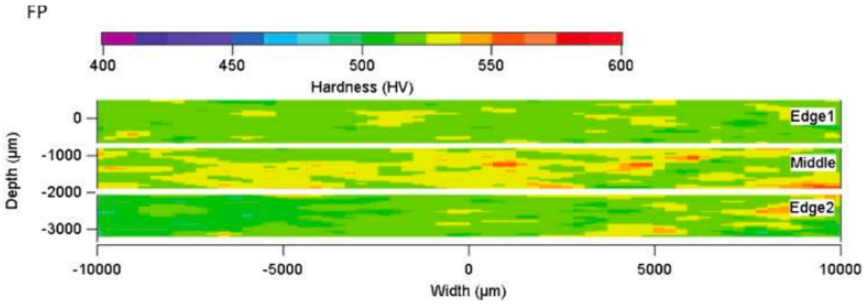


**Figure 3. Variability in through-thickness hardness of a Flash processed Fe-C-Cr steel. [3]**

Under rapid heating conditions, the austenite-start and austenite finish temperatures are influenced by the kinetics of carbide dissolution, austenite nucleation and growth, and are typically higher than the equilibrium values [4]. The dissolution environment of the carbides, and hence their dissolution kinetics are closely related to grain growth that occurs during the heating portion of the Flash thermal cycle. The dissolution of carbides at grain boundaries are influenced by the high-diffusivity grain boundary path while the dissolution of interior carbides is rate-determined by solute diffusion in the matrix. One of the objectives of the mesoscale simulations is to capture the deviation in phase equilibria as influenced by the Flash processing thermal cycle. The project approach involves use of mesoscale simulations using Monte Carlo (MC) to represent the initial polycrystalline grain structure prior to Flash processing, and to use phase field simulations in order to capture the coupled evolution of the carbide, ferrite, and austenite phases during the Flash thermal cycle. The computational objective of the project is to perform high-performance computing (HPC) based phase-field simulations of carbide dissolution, austenite nucleation and growth in a carbide + ferrite microstructure during Flash processing of an Fe-Cr-C steel using the Microstructure Evolution Using Massively Parallel Phase-field Simulations – Solid State (MEUMAPPS-SS) phase field code in order to capture the effect of the initial microstructure and the Flash thermal cycle on the concentration gradients developed at the mesoscale prior martensitic and / or bainitic transformations occurring in the microstructure upon further cooling to room temperature. The initial polycrystalline grain structure was obtained in certain cases using a three-dimensional MC simulation code that realistically captures the topology of grains. The carbide particles were then introduced into the three-dimensional grain structure.

## 2. RESULTS

The results obtained during this project for the various tasks presented in the statement of work (SOW) are presented in this section.

### 2.1 INTEGRATE FE-C AND FE-CR-C ALLOY THERMODYNAMICS INTO MEUMAPPS

**Objective**: Generate thermodynamic data for Fe-C and Fe-Cr-C for integration into MEUMAPPS.

**Progress:** MEUMAPPS phase field simulations require the Gibbs-free energies of a phase at a given temperature to perform quantitative simulations. The steel database TCFE9 in the ThermoCalc software was used to estimate thermodynamic properties of Fe-Cr-C ternary system. The Gibbs energies of ferrite, austenite, and carbide [$(Fe,Cr)_3C$] were fitted to a quadratic equation of the form,

$$G^{\phi} = A_1^{\phi}\left(x_{Cr} - A_4^{\phi}\right)^2 + A_{12}^{\phi}\left(x_C - A_5^{\phi}\right)^2 + A_3^{\phi} \quad [1]$$

where the A's are the fitting parameters shown in Tables 1-3. The free energies were calculated at temperatures ranging from 600°C to 1,100°C in steps of 50°C. The fitting parameters at any intermediate temperature were linearly interpolated using the tabulated parameters.

**Table 1. Gibbs free energy fitting parameters for the ferrite phase in Fe-Cr-C system**

| Temperature [°C] | $A_1$ | $A_2$ | $A_3$ | $A_4$ | $A_5$ |
|---|---|---|---|---|---|
| 600 | 1024576.9232 | 1823234.7137 | -34383.2227 | 0.02 | 0.0001 |
| 650 | 1120480.7694 | 1758443.4808 | -37518.6793 | 0.02 | 0.0001 |
| 700 | 1216625.0001 | 1695967.6466 | -40780.5693 | 0.02 | 0.0001 |
| 750 | 1313538.4617 | 1635844.9065 | -44174.2093 | 0.02 | 0.0001 |
| 800 | 1407182.6925 | 1578441.5267 | -47701.6914 | 0.02 | 0.0001 |
| 850 | 1495048.0771 | 1523015.2367 | -51340.5142 | 0.02 | 0.0001 |
| 900 | 1580067.3079 | 1469066.0765 | -55076.5929 | 0.02 | 0.0001 |
| 950 | 1663548.0771 | 1416515.5167 | -58901.5626 | 0.02 | 0.0001 |
| 1000 | 1745778.8463 | 1365147.5667 | -62809.3284 | 0.02 | 0.0001 |
| 1050 | 1827067.3079 | 1314815.6563 | -66795.2540 | 0.02 | 0.0001 |
| 1100 | 1907798.0771 | 1265472.2908 | -70855.7052 | 0.02 | 0.0001 |

The fitting range for Cr was $0 \leq X\_Cr \leq 0.02$ and for C $0 \leq X\_C \leq 0.03$ based on the equilibrium concentrations of Cr and C in ferrite with other phases in the temperature range of 600°C-1,100°C.

**Table 2. Gibbs free energy fitting parameters for the austenite phase in Fe-Cr-C system**

| Temperature [°C] | $A_1$ | $A_2$ | $A_3$ | $A_4$ | $A_5$ |
|---|---|---|---|---|---|
| 600 | 1163493.5899 | 485334.4945 | -33619.3358 | 0.02 | 0.0001 |
| 650 | 1241474.3591 | 483830.3595 | -37005.2257 | 0.02 | 0.0001 |
| 700 | 1319333.3335 | 482865.6057 | -40476.7374 | 0.02 | 0.0001 |
| 750 | 1397141.0258 | 482430.3301 | -44030.6460 | 0.02 | 0.0001 |
| 800 | 1474717.9489 | 482470.7422 | -47663.8453 | 0.02 | 0.0001 |
| 850 | 1552358.9745 | 483000.6265 | -51373.8079 | 0.02 | 0.0001 |
| 900 | 1630012.8207 | 483974.0968 | -55157.9617 | 0.02 | 0.0001 |
| 950 | 1707653.8463 | 485416.1073 | -59014.0972 | 0.02 | 0.0001 |
| 1000 | 1785416.6669 | 487282.6024 | -62940.1637 | 0.02 | 0.0001 |
| 1050 | 1863243.5899 | 489591.4724 | -66934.2678 | 0.02 | 0.0001 |
| 1100 | 1941294.8720 | 492298.1003 | -70994.6402 | 0.02 | 0.0001 |

The fitting ranges in the case of austenite were $0 \leq X\_Cr \leq 0.02$ and $0 \leq X\_C \leq 0.05$.

**Table 3. Gibbs free energy fitting parameters for the $(Fe,Cr)_3C$ phase in Fe-Cr-C system**

| Temperature [°C] | $A_1$ | $A_2$ | $A_3$ | $A_4$ | $A_5$ |
|---|---|---|---|---|---|
| 600 | 584497.98630 | 2101398.84335 | -29803.41096 | 0.08 | 0.25 |
| 650 | 607810.57502 | 2323916.37438 | -32798.82490 | 0.08 | 0.25 |
| 700 | 631512.63449 | 2553182.13234 | -35874.14721 | 0.08 | 0.25 |
| 750 | 655609.72622 | 2788879.09601 | -39025.52950 | 0.08 | 0.25 |
| 800 | 680107.74276 | 3030721.64017 | -42249.50105 | 0.08 | 0.25 |
| 850 | 705012.94441 | 3278451.20761 | -45542.91635 | 0.08 | 0.25 |
| 900 | 730331.97240 | 3531832.75739 | -48902.91224 | 0.08 | 0.25 |
| 950 | 756071.84770 | 3790651.81755 | -52326.87232 | 0.08 | 0.25 |
| 1000 | 782239.96128 | 4054712.01569 | -55812.39718 | 0.08 | 0.25 |
| 1050 | 808844.05952 | 4323832.99261 | -59357.27928 | 0.08 | 0.25 |
| 1100 | 835892.22690 | 4597848.62628 | -62959.48156 | 0.08 | 0.25 |

The fitting ranges in the case of cementite were $0 \leq X_{Cr} \leq 0.08$ and $0.2 \leq X_C \leq 0.3$.

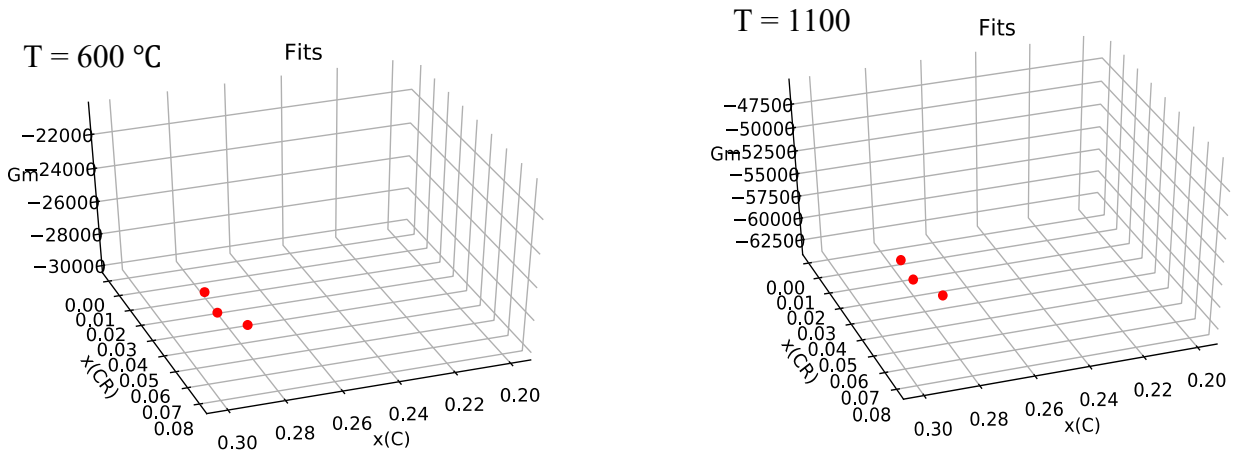


**Figure 4. Free energy surface for the cementite phase (blue) and values obtained using the fitting functions (red dots) at 600°C (left) and 1100°C (right).**

Figure 4 shows a comparison of the free-energy surface of the cementite phase obtained from ThermoCalc and the values obtained using the fitting functions shown in Eqn. 1.

## 2.2 EXTEND MEUMAPPS SIMULATIONS TO THREE-PHASE SYSTEMS

**Objective:** The objective of this task is to introduce modifications to the MEUMAPPS code to extend the capability of the two-phase Kim-Kim-Suzuki (KKS) model [5] to handle the potential coexistence of more than two phases.

**Progress:** The existing single-phase version of MEUMAPPS-SS was based on the KKS model. The basic assumption in the model is that the diffuse interface across two phases is made up of varying volume fractions of the solid and liquid phases whose compositions are such that the chemical potentials of the solute(s) are the same in the two phases. The single-phase KKS model was extended to multiple phases based on an approach presented by Zhou et al. [6]. Accordingly, the total chemical energy of the system consisting of austenite, ferrite, and cementite is defined as, where phase 1 is ferrite, phase 2 is cementite, and phase 3 is austenite.

$$G = \left[1 - \left(h(\phi_1)G^1 + h(\phi_2)G^2\right)\right] G^3 + h(\phi_1)G^1 + h(\phi_2)G^2 \quad [2]$$

where h is an interpolating polynomial for the free energy given by

$$h(\phi) = \phi^3\left(6\phi^2 - 15\phi + 10\right). \quad [3]$$

The total interfacial energy is given by

$$G^{int} = \omega^1\phi_1^2(1 - \phi_1)^2 + \omega^2\phi_2^2(1 - \phi_2)^2 + \omega^3\phi_3^2(1 - \phi_3)^2 \sum_{i=1}^{3}\sum_{j\neq i}^{3}\phi_i^2\phi_j^2 \quad [4]$$

where the first three terms on the right-hand side is the interfacial energy between the individual phases and the matrix, the second term is the interfacial energy between each of the 3 phases. A gradient energy is used to account for the energy penalty due to gradients in $\phi$ given by

$$G^{Grad} = 0.5\sum_{p=1}^{3} \nabla\phi_p^T \kappa^p \nabla\phi_p \quad [5]$$

where $\kappa$ is an anisotropic gradient coefficient. The interface between the phases is considered semi-coherent and the elastic energy contribution is assumed to be zero. The three phases considered here are the ferrite, austenite, and carbide.

The evolution equations solved are the time-dependent Ginzburg-Landau (TDGL) equation and the diffusion equation. TDGL is given by

$$\frac{\partial\phi_p}{\partial t} = -\frac{\mathrm{L}}{\tilde{N}}\sum_{p\neq q}^{\tilde{N}}\left(\frac{\delta G}{\delta\phi_p} - \frac{\delta G}{\delta\phi_q}\right) \quad [6]$$

where L is the phase field mobility and $\tilde{N}$ is the total number of variants that co-exist at any mesh point, and the $\delta$ on the right-hand side refer to functional derivatives. The above formulation of the TDGL satisfies the constraint that the sum of the $\phi$s at any point satisfies the condition $\sum_{p=1}^{N+1}\phi_p = 1$ at every mesh point. The diffusion equation is given by

$$\frac{\partial C_{Cr,C}}{\partial t} = \nabla.M_{Cr,C}\nabla\mu_{Cr,C} \quad [7]$$

where M is the mobility of Cr (or C) and $\mu$-s represent the chemical potentials of the species in each phase. KKS formulation requires the calculation of the Cr and C and concentrations at the various phase interfaces using the equal chemical potential assumption, $\mu_{Cr,C} = \frac{\partial 3}{\partial C^3_{Cr,C}} = \frac{\partial G^p}{\partial C^p_{Cr,C}}$, where p = 1 or 2. This requires the solution to M x N simultaneous equations where M is the number of solutes and N is the number of phases in the system. By representing the chemical free energies in the form quadratic equations described in Task 2, this leads to a system of linear equations. The evolution equations are solved using a semi-implicit Fourier spectral technique, which is well established in the literature [7].

## 2.3 PERFORM MEUMAPPS PHASE FIELD SIMULATIONS USING SINGLE PARTICLE EMBEDDED IN A SINGLE CRYSTAL OR BICRYSTAL

**Objective:** Perform phase field simulations to capture the dissolution of carbide, and nucleation and growth of austenite situated inside a grain or at a grain boundary with specified misorientation.

**Progress:** The following simulations were performed during the course of the project in support of Task 3. Initially, the simulations were focused on differentiating the dissolution behavior of carbides situated on the grain boundaries versus inside the grains. However, based on discussions with the industry and with subject-matter experts at the Oak Ridge National Laboratory (ORNL), it was decided to focus more on the intragranular precipitates. The initial results in the order in which they were carried out are presented involving grain boundaries and the results focusing just on the intragranular carbides are presented subsequently.

### 2.3.1 Grain boundary – Particle Interaction

The phase field model of Chang and Moelans [8] was implemented within MEUMAPPS-SS framework. Phase field simulations were performed using the test cases provided in the paper. The simulations were carried out in 3-D using up to 256 processes in the Titan supercomputer at ORNL. The results captured the interaction of a moving grain boundary with a dissolving particle, depending on the boundary velocity and the diffusion coefficient of the solute. Figure 5 summarizes the simulation results.

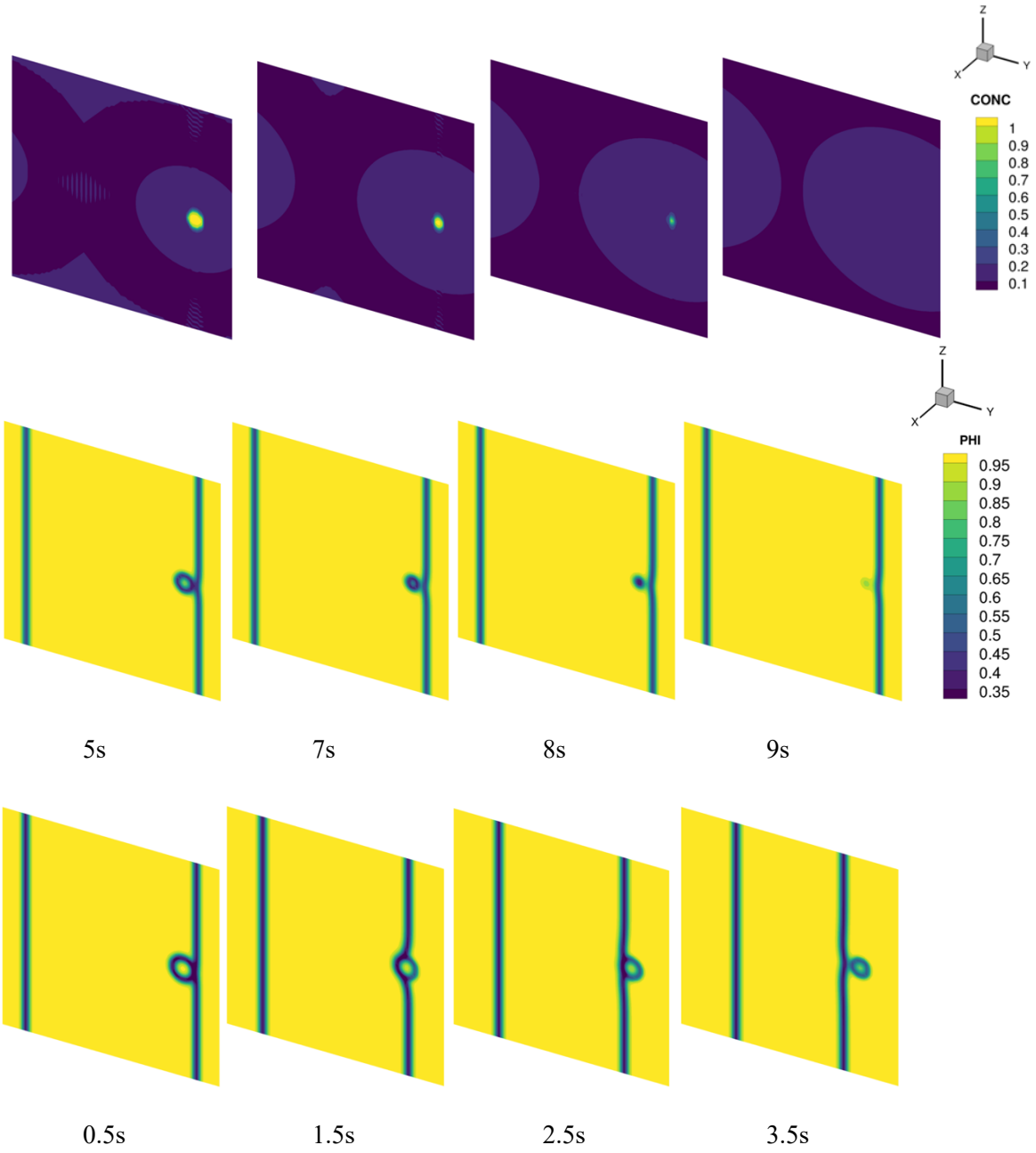


**Figure 5. Phase field simulations of the interaction of a moving grain boundary with a dissolving particle. When the solute has a high diffusion coefficient and when the boundary velocity low, there is sufficient time for the particle to fully dissolve. Solute Concentration profiles (top) and order parameter (middle) as a function of time. When the particle size and the grain boundary. velocity are increased, the grain boundary overcomes the particle. Order parameter profiles shown as a function of time (bottom).**

As shown in Figure 5, the interaction between a grain boundary and precipitate may lead to the complete dissolution of the precipitate when there is sufficient interaction time. However, there is no clear experimental evidence to show that such a phenomenon occurs during Flash processing.

### 2.3.2 Effect of variable solute diffusion coefficient

The simulations shown in Figure 5 were performed using isotropic diffusion coefficient. Therefore, the concentration gradients developing at dissolving particles were identical (spherical) whether the particle was situated at a grain boundary or inside the grains. In order to account for the effect of more rapid diffusion along the grain boundary, the methodology proposed in [9] was implemented within the Fourier spectral approach used to solve the Cahn-Hilliard equation. The modified phase field simulations were applied to the interaction between particle and grain boundary assuming an enhanced pipe diffusion at the grain boundary. A model for solute diffusivity was introduced that allowed local diffusion coefficient to be defined in terms of the prevailing order parameters. Such formulation allowed diffusion coefficient in the grain boundary regions to be enhanced by four orders of magnitude compared to the bulk. For the current simulations, a non-dimensional form of the evolution equation was used in order to test the model. Nevertheless, the results show that under certain conditions, the dissolution of grain boundary carbides can lead to preferential solute diffusion along grain boundaries resulting in solute segregation along grain boundaries. The situation was captured for two different simulation conditions: (1) a single grain boundary precipitate situated along a flat boundary, shown in Figure 6, and (2) multiple precipitates intersecting a shrinking spherical grain shown in Figure 7. Because of the vast difference in the diffusion coefficient of the solute between the bulk and the grain boundaries, a limitation is placed on the time step that can be used in the simulations even though the solution of the evolution equations used an implicit time-stepping approach. Extending the approach to a polycrystalline grain structure requires a significant computational effort because of the increased number of order parameters.

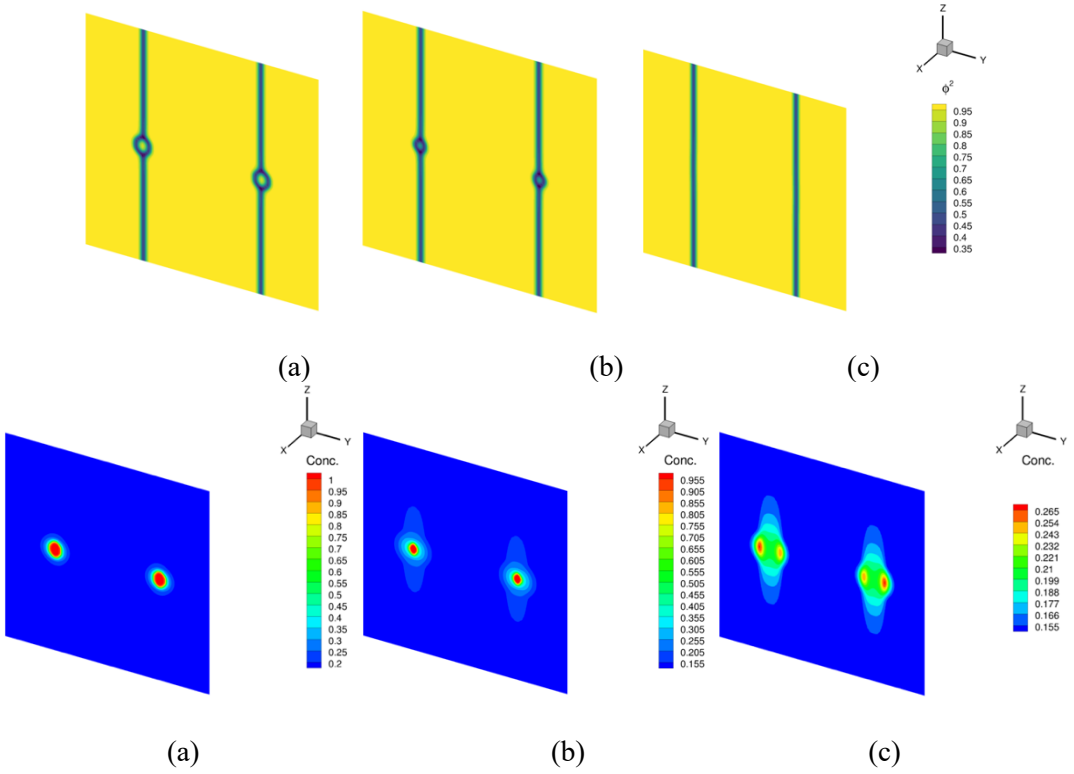


**Figure 6. Evolution of order parameter (top) and concentration field (bottom) during dissolution of a precipitate placed on a straight grain boundary. Preferential spreading of solute along grain boundary plane (a) t=37.5 (b) t=57.5 and (c)t=100.0.**

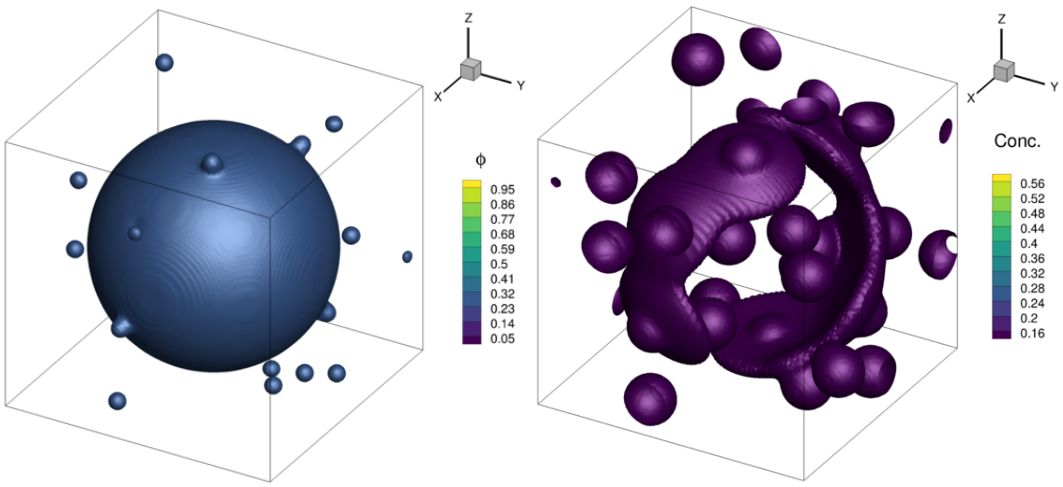


**Figure 7. Coupled evolution of a circular grain intersecting a number of soluble precipitates. (a) initial configuration and (b) Formation of enriched solute layer along the circular grain boundary during dissolution of precipitates intersecting the circular grain.**

The simulations so far have used model binary systems and model parameters that were chosen arbitrarily to demonstrate the feasibility of the phase field simulations for simulating grain boundary carbides and intragranular carbides with respect to their dissolution rates, and also the shape of the solute field due to dissolution. Before extending these models to the Fe-Cr-C system and for the thermal conditions typical of the Flash process, several meetings were held between the lab PI and the industrial PI, along with subject matter experts at ORNL who were involved in the characterization of the Flash processed samples at ORNL. Based on these discussions, it was evident that under Flash thermal conditions, the differences between the behavior of intragranular and intergranular carbides were minimal. Therefore, it was suggested that subsequent simulations be performed in single crystals, connecting more closely with the alloy thermodynamics and the thermal conditions of the Flash process. More emphasis was placed on the formation of austenite at the ferrite-carbide interface, the subsequent dissolution of the carbide in the austenite and the diffusion of carbon in the growing austenite field during the Flash thermal cycle. The simulations shown below are focused on single crystal domains containing an initial distribution of carbide particles.

### 2.3.3 Phase transformations during continuous heating

Simulations were performed for a domain consisting of a ferrite matrix containing a spherical particle of cementite. Simulations were performed in a 120 x 120 x 120 mesh with a spatial resolution of 2 x 10-9 m. The alloy composition was Fe-0.01Cr-0.05C (atom fractions). A constant interfacial energy of 0.3 J/m2 was used for the interface energy between the phases. The simulations were run using Summit supercomputer at ORNL. The thermodynamic fits described under Task 1 were used to describe the free energies of phases as function of temperature. The initial microstructure was allowed equilibrate at 750° C. It was then heated from 750°C to 1,100°C at 10°C/s or 100°C/s and cooled at the same rate to 600°C. A thin layer of the austenite phase was placed at the ferrite-carbide interface with same concentration as ferrite at different temperatures above the A1 temperature (equilibrium temperature at which austenite field is encountered for the average composition of the alloy). The evolution of the austenite phase under the different heating conditions was monitored. Carbon diffusion in Fe-Cr ferrite as a function of concentration and temperature was modeled using the approach proposed by Vasilyev [10]. C diffusion in Fe-Cr austenite was modeled using the approach of Lee et al. [11]. Figure 8 shows the behavior of austenite placed at the ferrite-carbide interface at 850°C for a heating rate of 10°C/s. It shows the

complete dissolution of carbide in the austenite phase around 880°C upon heating. The austenite phase continued to grow and consumed the ferrite on heating to 1,100°C and during cooling following the peak temperature of 1,100°C.

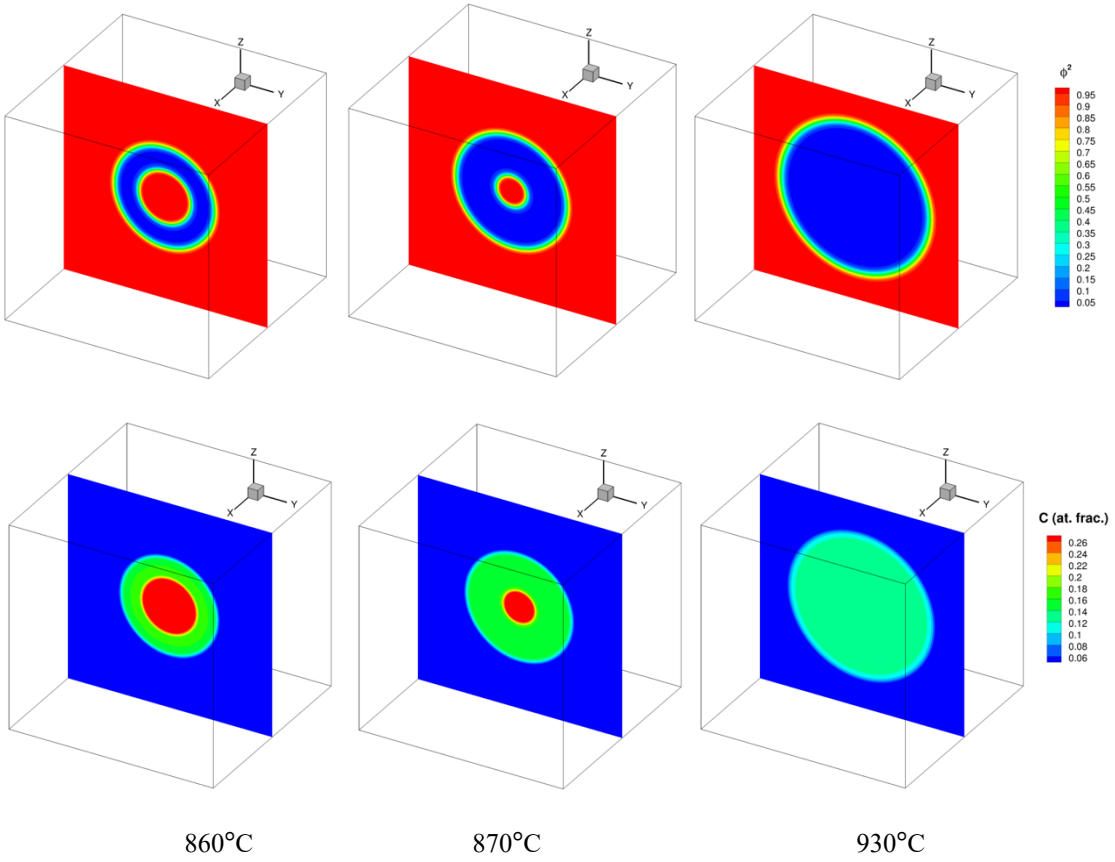


**Figure 8. Simulations of austenite nucleation and growth (blue phase in the top row) and the evolution of austenite carbon content (green in bottom row) during heating at 10°C/s. At this low heating rate austenite nucleation and carbide dissolution ae completed during the heating portion.**

The carbon centration profiles across the carbide-austenite-ferrite phases at various temperatures upon heating to 930°C at heating rates of 10°C/s and 100°C/s are shown in Figure 9 for the austenite rim introduced at 850°C. While for the heating rate of 10°C/s complete dissolution of carbide in austenite (full austenitization) occurs around 890°C, the carbide dissolution in austenite is insignificant at the same temperature (930°C) when heated at 100°C/s. Complete dissolution of carbide in austenite and the subsequent expansion of the austenite phase leads to a reduction in the maximum carbon content in the austenite phase that enhances its chances of transforming to bainite or martensite during cooling to room temperature. However, if the austenite phase does not have time to evolve during the thermal cycle, it has the potential to remain as thin films of retained austenite on cooling to room temperature. Such austenite regions are considered to have a significant effect on the ductility of the Flash processed steels.

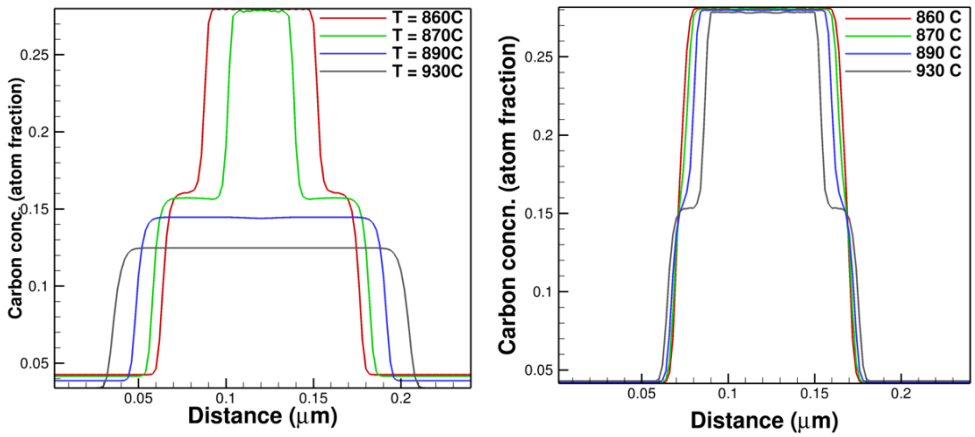


**Figure 9. Effect of heating rate on austenite nucleation and carbide dissolution kinetics. (a) and (b) show the carbon concentration. At 10°C/s (a) an austenite nucleus placed at the ferrite-carbide interface at 850°C consumes the carbide completely around 890°C. However, at 100°C/s, the austenite has hardly grown, and the carbide dissolution is negligible upon heating to 930°C.**

The kinetics of carbide dissolution in austenite under the two heating rates shown is in Figure 10 where the maximum concentration of carbon in the simulation domain is plotted as a function of temperature, on heating to the peak temperature of 1,100°C, and on subsequent cooling at the same rate to 600°C . At 10°C /s, the maximum carbon concentration drops suddenly when the carbide dissolves completely (around 890°C on heating) and continues to drop upon continued heating to 1,100°C and cooling to 600°C . However, at 100°C /s, the evolution is much sluggish as expected. Austenite introduced at 850°C completely dissolves the carbide only around 1,080°C during heating (complete austenitization), while austenite introduced at 900°C and 950°C dissolve only on cooling around 1,070°C and 1,030°C, respectively. The results were presented at The Metals, Minerals and Materials Society (TMS) Annual Meeting at San Diego, June 2020 [12].

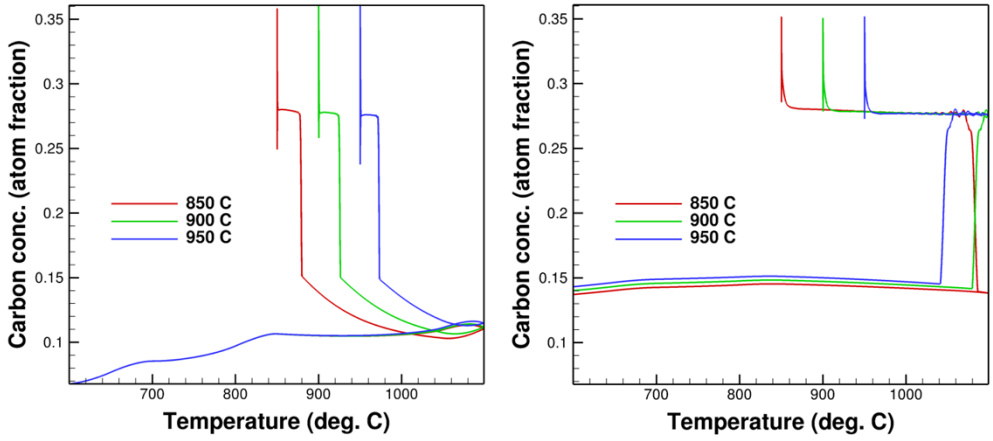


**Figure 10. C concentration versus temperature on heating at cooling at 10°C /s (left) and 100°C /s (right).**

### 2.3.4 Microstructure Evolution under typical Flash thermal cycles

After establishing some of the fundamental aspects of austenite nucleation and growth kinetics as a function of heating rate, microstructure evolution simulations were performed using actual Flash thermal profiles obtained from the industry. The simulations were performed for 8620 (Fe-Cr-C) steel. The

composition of the steel was Fe-0.008Cr-0.02C. The Flash thermal cycle used in the simulations is shown in Figure 11. The initial heating rate to the peak temperature is roughly 300°C /s up to about 900°C after which it drops significantly up to the peak temperature of 990°C . This is followed by an initial cooling period of about 1.5s during which the cooling rate is extremely slow, roughly 20°C /s.

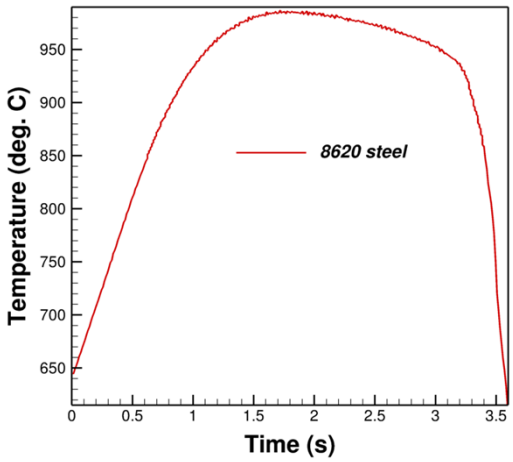


**Figure 11. Typical Flash thermal cycle used in the simulation of 8620 steel.**

### 2.3.4.1 Single Carbide

MEUMAPPS simulations were performed with a single carbide particle at the center of the simulation domain of 120 x 120 x 120 points with a spatial resolution of 0.1 nm. Two different carbide sizes were simulated using sizes of 0.1 $\mu$m or 0.25 $\mu$m. The 0.1 $\mu$m carbide dissolved completely during the above Flash thermal cycle, while the 0.25 $\mu$m carbide remained undissolved after the thermal cycle. The simulations results are shown in Figure 12. These results were compared against experimental measurements of carbide size distribution after the Flash treatment. As will be shown later, the simulation results are consistent with the experimental measurements.

### 2.3.4.2 Multiple Carbides

The MEUMAPPS simulations were performed using a domain of 126 x 126 x126 points. Multiple Carbide precipitates were randomly introduced inside the cubic domain. The size of each isolated carbide is 0.05 micrometer. The smaller carbide size was used in order to accommodate multiple carbide particles in a reasonable simulation volume. Overlap of particles led to particles with elongated shapes during early part of the evolution as shown in Figure 13.

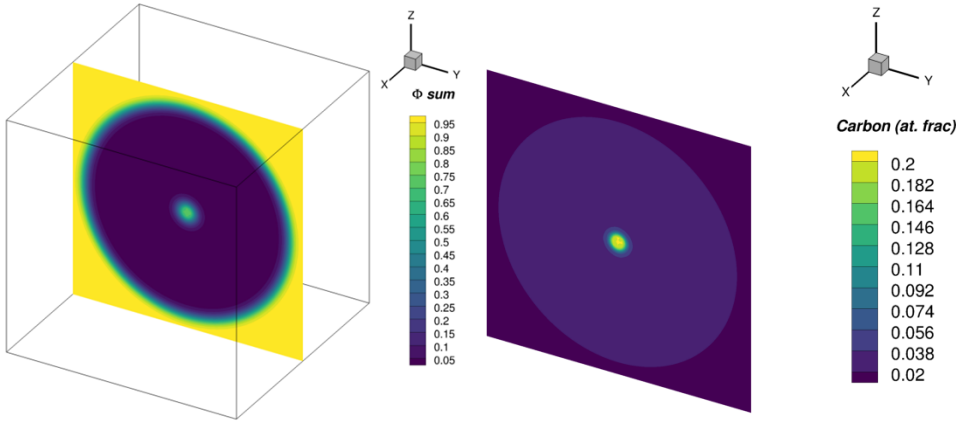

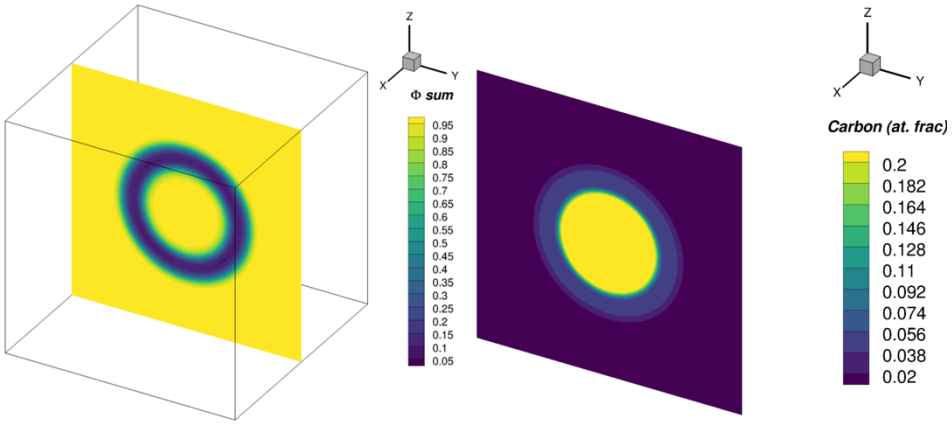


**Figure 12. Evolution of a single spherical carbide during Flash thermal cycle. 0.10 µm carbide fully dissolves (top) while 0.25 µm carbide remains undissolved at the end of the thermal cycle.**

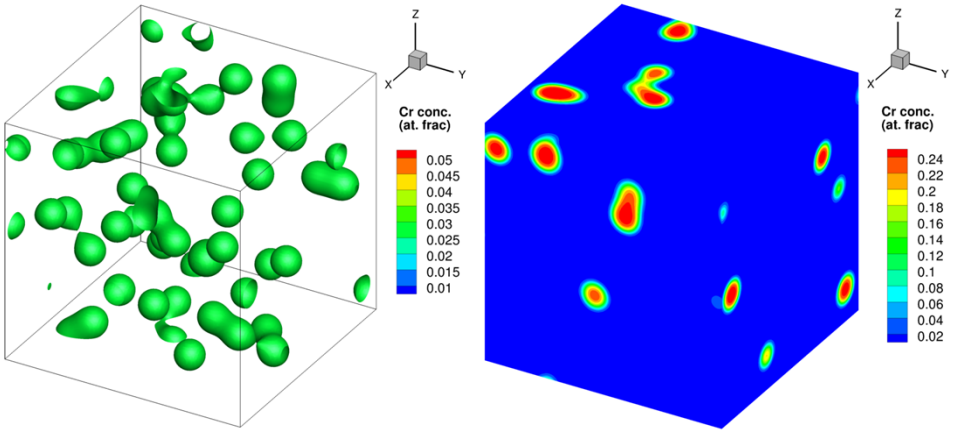


**Figure 13. Initial microstructure showing distribution of carbide particles.**

The microstructure evolution during the Flash thermal cycle shown in Figure 14 was simulated using MEUMAPPS. The simulations evolved both the C and Cr concentrations as well as the order parameter corresponding to the carbides.

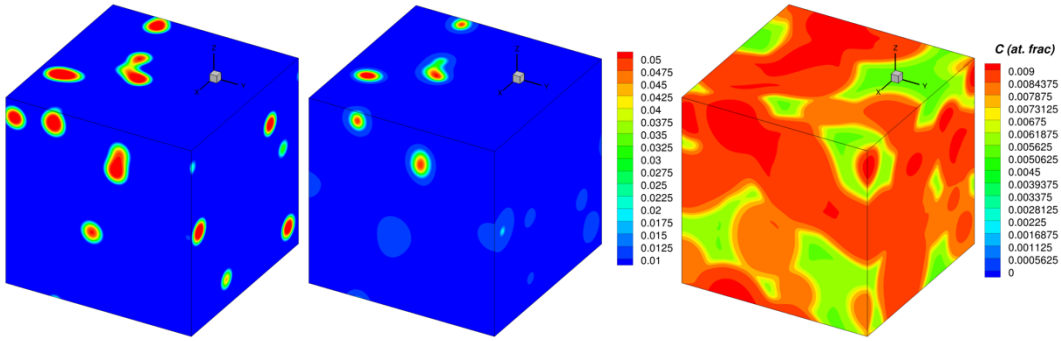

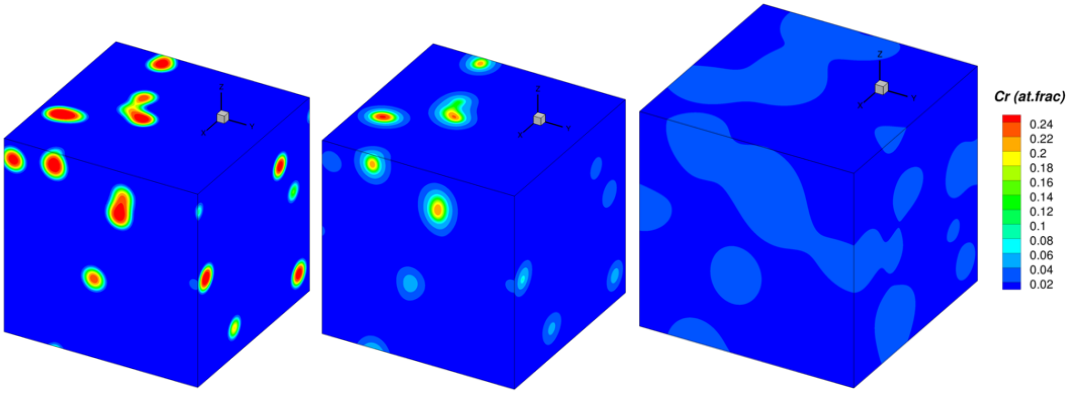


T=649°C T=981°C T=615°C (on cooling)

**Figure 14. Evolution of carbon concentration profiles (top) and Cr concentration profiles (bottom) during Flash thermal cycle shown in Figure 11.**

Figure 14 shows that the 0.05 $\mu$m sized carbides completely dissolve during the Flash thermal cycle. The Cr and C concentration profiles at the end of the thermal cycle at 615C on cooling capture the microstructure of the steel prior to the onset of the bainitic/martensitic transformation. Although this is not explicitly modeled in the current simulations, thermodynamic calculations can be performed independently to assess the transformation behavior of these regions on cooling to room temperature.

Based on discussions with one of the industry collaborators who provided the Flash thermal cycle [13], the carbide sizes in the 8620 steel are somewhat larger, in the 0.3 to 0.6 micrometer range. The initial distribution of the carbides in microstructure of the steel after Flash processing, and the corresponding carbide size distribution are shown in Figure 15[13]. Bin sizes for the histograms are 0.1 $\mu m^2$ for the area and 0.1 µm for the equivalent diameter graphs. The fit curves are log normal. It appears that the majority of precipitates (as seen in this magnification) are between 0.3 to 0.6 µm in size. The size of carbides in the starting material would then be a bit larger.

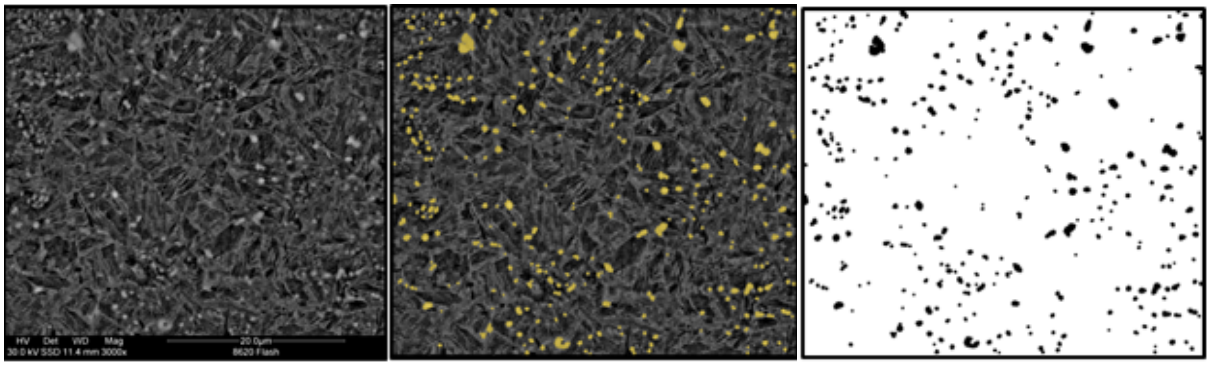

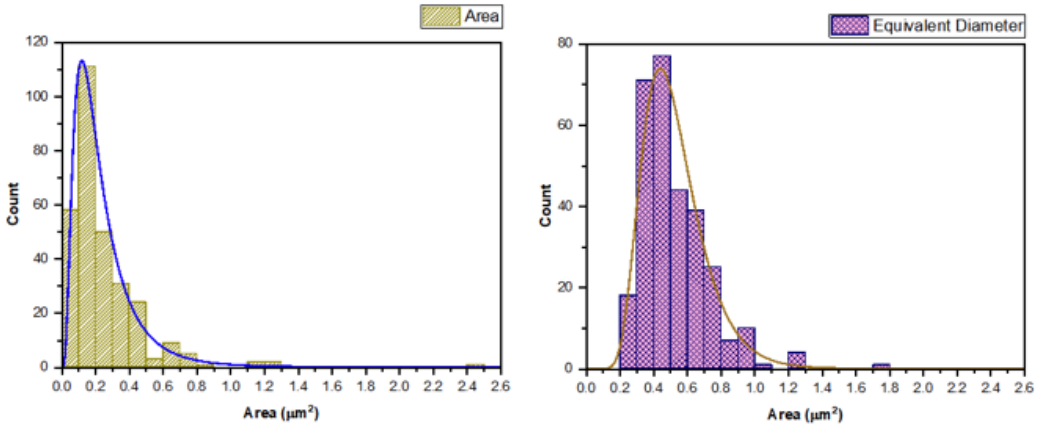


**Figure 15. Image processing of AISI 8620 steel after Flash processing (top), and distribution of carbide area and size distribution (bottom).**

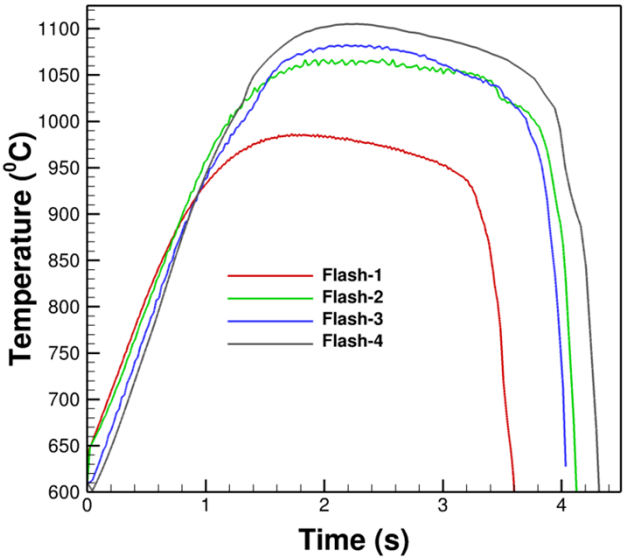


**Figure 16. Flash thermal cycles used to simulate carbide evolution.**

Figure 15 shows that the count of carbide particles below about 0.1 μm is close to zero, which agrees with the simulations shown above. Additional Flash thermal cycles with different peak temperatures and total duration of the Flash thermal cycle used in 8620 steel experiments were obtained and phase field simulations of carbide evolution were performed using a larger carbide size. The thermal cycles used in the simulations is shown in Figure 16, and carbide evolution during Flash-2 thermal cycle is shown in Figure 17.

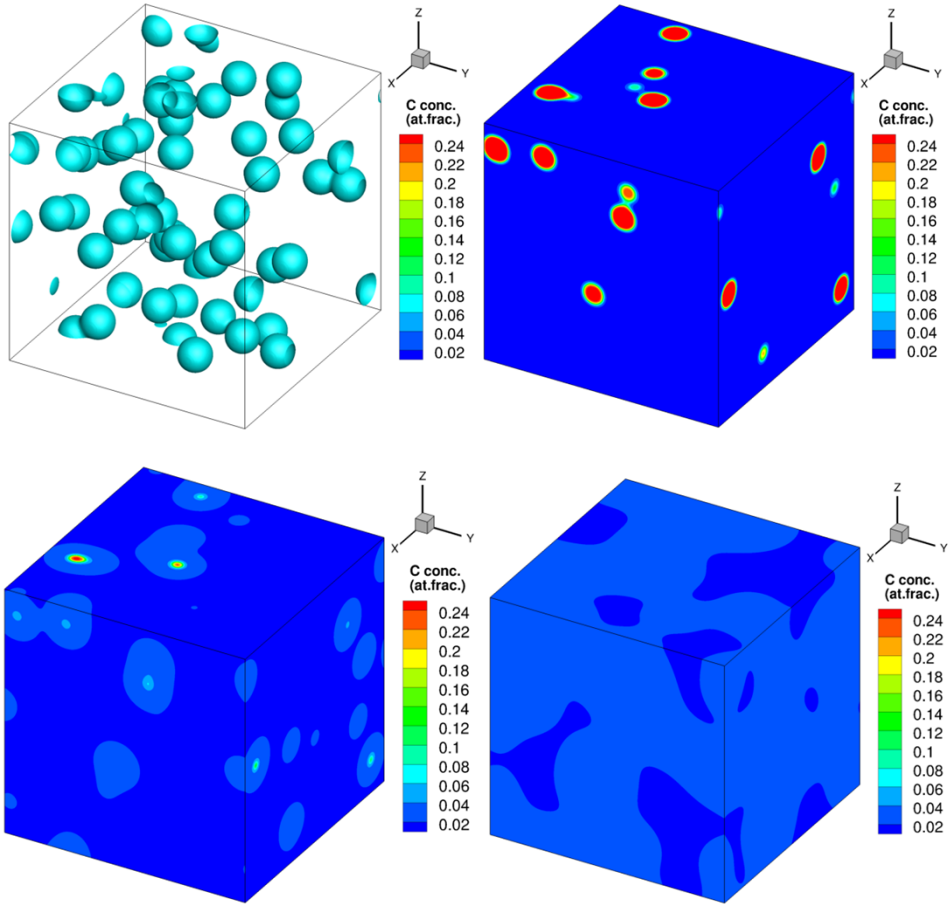


**Figure 17. Evolution of carbon concentration due to phase evolution and diffusion during Flash-2 thermal cycle.**

The initial carbide particle size shown in the top left image is 0.10 µm. From Figure 17, the following observations can be made. It is clear that practically no microstructure evolution occurs on heating from 650°C to 900°C . In all of these above simulations using different Flash thermal cycles, the austenite rim, as described previously, was inserted at an on-heating temperature of 850°C . It is clear that the austenite does not show any evolution after it is heated to 900°C as shown in the top right image. The microstructure at 1,060°C , corresponding to the peak temperature in the Flash-2 thermal profile shows a mixture of residual carbide and a growing rim of austenite with a carbon concentration of roughly 0.05. Upon progressing through the thermal cycle, the carbides are fully consumed, and austenite field expands to cover the simulation volume almost entirely as shown in the bottom right Figure 17.

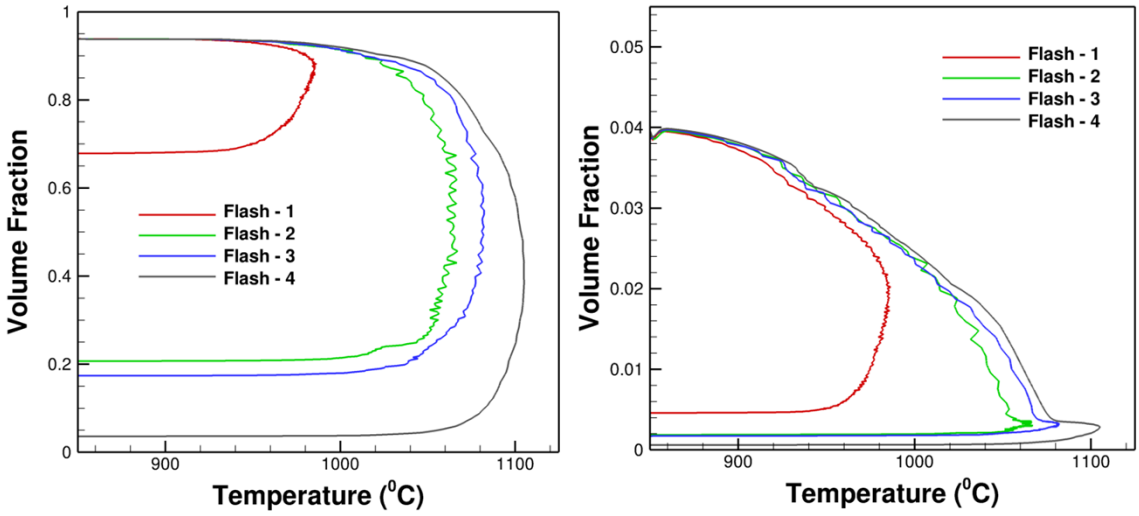


**Figure 18. Volume fraction of ferrite (left) and carbide (right) as a function of temperature during Flash thermal cycles 1-4.**

Figure 18 shows the evolution of the volume fractions of ferrite and the carbide as a function of temperature during the various Flash cycles. The effect of thermal cycle on the evolution of the microstructure is captured quantitatively in Figure 18. For example, the volume fraction of ferrite remains almost constant until the volume fraction of austenite that forms at the interface between the carbide and ferrite starts to grow significantly. It is clear that for the Flash-1 thermal cycle, only about 30% of the simulation volume is consumed by the growing austenite. The volume fraction of carbide goes down from an initial value of roughly 4% to about 0.05% at the end of the thermal cycle, indicating that the dissolution of carbides in austenite is not complete. However, for Flash cycles 2-4, more and more austenite are formed due to the faster diffusion kinetics at higher temperatures and dwell times experienced compared to the Flash-1 thermal cycle. Flash-4 thermal cycle with the highest peak temperature and the longest dwell time has the lowest amount of residual ferrite. The ferrite volume fraction does not go to zero because in a diffuse interface model such as phase field, the volume fraction of a phase at any point varies continuously from 0 to 1. Therefore, small residual non-zero order parameter corresponding to ferrite at any location gets added to the total volume fraction.

## 2.4 PERFORM LARGE SCALE MC SIMULATIONS OF GRAIN STRUCTURE EVOLUTION WITH EVOLVING CARBIDES

**Progress:** These simulations were performed using a model binary alloy at a constant temperature. Because of the change in focus and the difficulties associated with anisotropic diffusion along grain boundaries, the simulations were not extended to the target Cr-C steel and to continuous heating and cooling conditions existing in a Flash thermal cycle. The phase field framework Chang and Moelans [8] was extended to a polycrystalline grain structure consisting of dissolving second phase particles. The simulations were carried out in 3-D using up to 256 processes in SummitDev supercomputer. The simulation volume consisted of 130 grains and had about 5% by volume of a dissolving second phase introduced in the form of clusters. A MC technique was used to develop the initial grain structure and was provided as input to the phase field code. Typical results are shown in Figure 19. Significant particle dissolution was observed as a result of annealing, associated with concomitant grain growth. However, as mentioned previously, according to experimental evidence significant dissolution of carbides on grain boundaries does not occur under Flash thermal cycling for Fe-C-Cr steels. Significant modifications to

MEUMAPPS is required in order to handle multiple grain simulations under Flash conditions for ternary alloys.

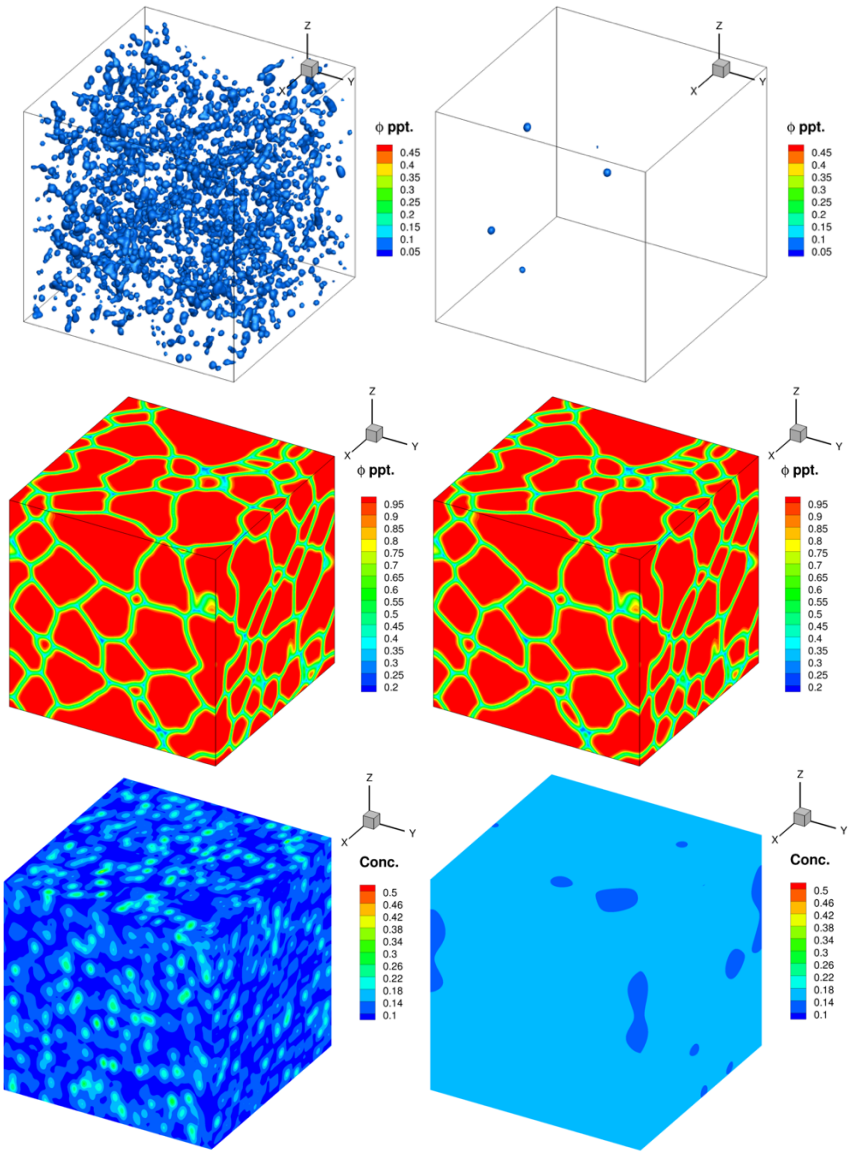


**Figure 19. Phase field simulations of the interaction of grain boundaries with a dissolving-particles in a polycrystalline structure showing the dissolution of the particles (top), evolution of grain structure (middle) and the evolution of the solute concentration field (bottom) in a model binary alloy.**

## 3. DISCUSSION

The simulations performed in this project can be classified into two different sets. The first set involved simulations of the interaction of carbide particles and grain boundaries using model alloys and model phase-field parameters. These simulations were performed at the bi-crystal, and polycrystal scales, using either isotropic or anisotropic diffusion coefficients for the solute. For the case of bicrystals with isotropic diffusion coefficient, two extreme cases were shown – (a) the presence of a slow-moving rain boundary

and a fast-diffusing solute results in complete dissolution of the carbide particle, while (b) for the fast-moving grain boundary the dissolution, the contact time between the carbide and boundary is not high enough to achieve complete dissolution. The driving force for the movement of the straight boundary was systematically varied in the simulations using a model parameter. However, for a polycrystalline grain structure, the boundary velocity is inversely proportional to the grain size. It appears that for the grain sizes used in the polycrystalline structure, the driving forces are low enough that the high residence time between the carbide particles and curved grain boundaries for sufficient to cause almost complete dissolution of the particles. In order to extend the simulations to real alloys using realistic alloy and interfacial properties would require an enormous computational cost which would be prohibitive even using the HPC facilities. By using an anisotropic diffusion coefficient with an enhanced diffusivity along grain boundaries, it was shown that the diffusion field became non-circular with enhanced penetration of solute along the grain boundaries. However, in order to relate such effects realistically to real polycrystals in alloys requires further physics input and much higher computational effort. Also, based on the discussions with experimental collaborators of the industry PI, it was decided that the behavior of the intragranular carbides was more critical in determining the final volume fractions of the various phases that coexist at room temperature after Flash processing. Therefore, further simulation effort was focused on single crystals containing multiple carbide particles.

The modified MEUMAPPS code with multiple-phase capability is clearly demonstrated by the ability to handle the co-evolution of carbide, austenite, and ferrite. The simulations are able to capture the experimental observation that the nucleation and growth kinetics of austenite at the ferrite-carbide interface is controlled by the heating rate. The current simulations indicate that very little austenite growth occurs during the initial rapid heating phase of the Flash thermal cycle up to temperature of roughly 900°C , which is well above the Ac1 temperature of the steel. At high heating rates, complete dissolution of carbide in austenite does not occur even after a super heat of several hundred degrees centigrade. This agrees with experimental findings of Flash heat treatments performed on 8620 steels [13]. Finally, the simulations have been extended to simulation volumes in which a statistically significant number of carbide particles can be accommodated. The evolution equations are able to handle the vast differences in the diffusion coefficients of Carbon and Chromium and the temperature dependence of the diffusion coefficients. However, in order to carry the physics to length scales involving multiple grains it is estimated that problem sizes that are roughly three orders of magnitude larger at a minimum would be required.

The present phase field simulations do not include the final transformation of the inhomogeneous austenite to bainite or martensite. However, the output microstructures obtained from the phase field simulations consisting of austenite with known concentrations of Cr and C can be used as input to thermodynamic and kinetic models based on packages such as JMatPro to calculate the potential for bainite / martensite formation based on the prevailing cooling rate.

## 3.1 IMPLEMENTATION

The implementation of the project proceeded according to the tasks listed in the SOW with some minor and major changes. The differences are explained below for each task.

- Integrate Fe-C and Fe-Cr-C alloy thermodynamics into MEUMAPPS – the task was completed as stated without any required modifications. The implementation into MEUMAPPS is well demonstrated by the results presented.

- Extend MEUMAPPS to simulation of three-phase systems - The task was completed without any issues. The strategy used for extending the code has been documented clearly in the report. The

implementation of the multi-phase code has been demonstrated by simulating the nucleation and growth of austenite from the ferrite-carbide interface.

- Perform MEUMAPPS phase field simulations using single particle embedded in single crystal or bicrystal - The task was completed without any issues. The single crystal simulations were performed both using single and multiple carbide particles using actual Flash thermal cycles obtained from the industry. The simulation results were in agreement with respect to the dissolution behavior of carbides under Flash thermal cycles. Characterization results involving particle size distribution after Flash processing in 8620 steel were used to validate the simulated dissolution behavior under Flash conditions. One of the changes from the SOW was regarding bicrystal simulations. The bicrystal simulations that were performed were based on ideal binary alloy and ideal input parameters and not for the Fe-Cr-C alloy. However, the simulations did capture some of the basic findings reported for the binary alloy bicrystals. Further development of the MEUMAPPS code was required to extend it to bicrystals and polycrystals. The focus of the simulations was shifted to the behavior of intragranular carbides after discussion with the PIs experimental collaborators at ORNL.

- Perform large scale MC simulations of grain structure evolution with evolving carbide particles - The intended workflow for this task was to first calculate the dissolution kinetics of grain boundary carbides under various grain environments and then use a reduced dissolution model for grain boundary precipitates as input to MC grain growth simulations in polycrystals. However, as mentioned earlier there were several decision points that resulted in a change in completing the task. (1) Significant modification of the MEUMAPPS code was required in order accurately incorporate grain boundary carbide interactions, (2) implementation of the phase field methodology to bicrystals with interacting precipitates using model alloys indicated a potential numerical issue associated with the orders of magnitude enhancement of the solute diffusion in the vicinity of the grain boundary, and (3) the focus of the effort was changed to the behavior of intragranular precipitates because there was no significant observed grain growth following Flash thermal cycle.

- Experimental support to mesoscale simulations - Some changes were necessary because of the shift in focus from polycrystals to single crystals. The industry provided information on different Flash thermal cycles that were used in Flash processing of the 8620 steel as well as the subsequent characterization of the processed microstructures. Several EBSP images of Flash processed 4140 steel were obtained from the industry that provided the input to the MEUMAPPS single crystal studies.

### 3.2 ISSUES OR CHALLENGES

One of the issues is related to the direct validation of the simulated concentration gradients at microscopic length scales using experimental measurements. Composition gradients in Carbon are masked at room temperature by the subsequent transformation to bainite / martensite. Therefore, there is an indirect way of validating the carbon distribution, by characterizing the volume fractions of bainite, martensite and retained austenite and comparing it with the computed volume fractions of the phases in the simulated microstructure. However, in order to perform such a comparison, it is necessary to use thermodynamic and kinetic models to compute the transformation kinetics of locations with different carbon (and Cr) contents in the simulated austenite. It was not possible to perform such calculations since it was beyond the scope of the SOW. However, we did compare the dissolution kinetics of carbide during different Flash thermal cycles obtained using the simulations experimental measurements and found a qualitative agreement. Another issue was related to the simulation of grain structure evolution in large polycrystalline microstructures as influenced by the dissolution of grain boundary carbides. We ran into a numerical difficulty while simulating the evolution of grain boundary carbides when the grain boundary diffusivity was orders of magnitude larger than bulk diffusivity. The time step in the phase field simulations had to be significantly reduced in order to perform such simulations. Extending the

simulations to multiple grains would have been impossible given the computational load associated with reduced time step. However, we did simulate the interaction between carbides and grain boundaries in a polycrystal using isotropic diffusion coefficient and found that most of the initial carbide precipitates dissolved during grain growth in a model binary alloy.

### 3.3 FUTURE WORK

Current processing activities at Flash Steelworks are focused on improving the throughput of the Flash processed steels by reducing cycle time by an order of magnitude. This not only involves challenges on the operational side but also required more extensive research in trying to quantify the microstructural evolution during extremely rapid heating and cooling cycles involved in the process. The PI has initiated discussions on how best to utilize the modeling capability developed as part of the current project to contribute to better understanding and optimization of the high-throughput Flash processing cycles. The current modeling tool has the potential to accurately predict local compositions and composition gradients arising from rapid heating and cooling. The results of these simulations can be combined with future thermodynamic and kinetic modeling to predict the formation of bainite/martensite or the retention of the austenite phase in the microstructure on cooling to room temperature. Another important follow-up work is to utilize the output of the microstructure predictions with existing multi-phase crystal plasticity frameworks developed at ORNL to understand microstructure-property linkages in heterogeneous materials such as Flash processed steels that show exceptional combinations of strength and ductility

## 4. REFERENCES


1. C. H. Young and H. K. D. H. Bhadeshia, “Strength of Mixtures of Bainite and Martensite,” Mater. Sci. Technol. 10, 209-214 (1994).
2. https://www.nextbigfuture.com/2015/12/super-strong-flash-bainite-steel.html
3. T. Lolla, G. Cola, B. Narayanan, B. Alexandrov and S. S. Babu, “Development of rapid heating and cooling (flash processing) process to produce advanced high strength steel microstructures,” Materials Science and Technology, 27, 863-875 (2011).
4. R. C. Reed et al., “Determination of re-austenitization kinetics in a Fe-0.4C steel using dilatometry and neutron diffraction,” Materials Science and Engineering, A256, 152-165 (1998).
5. S. G. Kim, W.T. Kim and T. Suzuki, “Phase-field model for binary alloys,” Phys. Rev. E., 60, 7186-7197 (1999).
6. N. Zhou et al., “Computer simulation of phase transformation and plastic deformation in IN718 superalloy: Microstructural evolution during precipitation,” Acta Mater. 65, 270-286 (2014).
7. L. Q. Chen and J. Shen, “Applications of semi-implicit Fourier-spectral method to phase field equations,” Comp. Phys. Comm. 108, 147-158 (1998).
8. K. Chang and N. Moelans, “Phase-field simulations of the interaction between a grain boundary and an evolving second-phase particle,” Philosophical Magazine Letters, 95, 202-210 (2015).
9. J. Zhu, L. Q. Chen, J. Shen and V. Tikare, “Coarsening kinetics from a variable-mobility Cahn-Hilliard equation: Application of a semi-implicit Fourier spectral method,” Phys. Rev. E, 60, 3564-3572 (1999).
10. A. A. Vasilyev and P. A. Golikov, “Carbon Diffusion Coefficient in Alloyed Ferrite,” Materials Physics and Mechanics 39, 111-119 (2018).
11. S. J. Lee, D. K. Matlock and C. J. Van Tyne, “An empirical model for carbon diffusion in austenite incorporating alloying element effects,” ISIS International, 51, 1903-1911, 2011.

12. B. Radhakrishnan, Y. Song and G. Cola, “Carbide dissolution during rapid thermal cycling of an Fe-Cr-C Steel,” TMS 2020, San Diego, California.
13. T. Lolla, The Ohio State University, internal communications.

## ACKNOWLEDGMENTS

This research was supported by the High-Performance Computing for Manufacturing (HPC4Mfg) program sponsored by the Advanced Manufacturing Office of the U.S. Department of Energy (DOE), and by the Exascale Computing Project (17-SC-20-SC), a collaborative effort of the U.S. DOE Office of Science and the National Nuclear Security Administration. This research used resources of the Oak Ridge Leadership Computing Facility, which is a DOE Office of Science User Facility supported under contract DE- AC05-00OR22725. Research performed at the Oak Ridge National Laboratory (ORNL), managed by UT-Battelle, LLC, under Contract No. DE-AC05-00OR22725 for the U.S. DOE.